Atomic structure of pyramidal defects in Mg-doped GaN

P. Vennégues,[1,*] M. Leroux,[1] S. Dalmasso,[1] M. Benaissa,[2] P. De Mierry,[1] P. Lorenzini,[1] B. Damilano,[1] B. Beaumont,[3] J. Massies,[1] and P. Gibart[3]

[1]*Centre de Recherche sur l'Hétéro-Epitaxie et ses Applications-CNRS-CRHEA, Rue Bernard Grégory, 06560 Valbonne, France*

[2]*CNRST, Bd Omar Ibn Khattab, Rabat, Morocco*

[3]*Lumilog, 2720 Chemin St. Bernard, 06220 Vallauris, France*

(Received 14 April 2003; revised manuscript received 5 August 2003; published 31 December 2003)

A detailed transmission electron microscopy study of pyramidal defects appearing in highly Mg-doped GaN is reported. It is shown that these defects are closed pyramidal inversion domains. From a high-resolution microscopy study, we propose atomic models for inversion domain boundaries which consist of Mg_3N_2 building blocks for both the basal and inclined facets of the pyramids. In Mg-doped GaN grown by metalorganics vapor phase epitaxy, these pyramidal inversion domains are a few nanometers wide, and their density is high enough to play a role in the free hole density decrease at high Mg doping.

DOI: 10.1103/PhysRevB.68.235214 PACS number(s): 61.72.Vv, 68.37.Lp, 78.55.Cr

I. INTRODUCTION

Gallium nitride is naturally *n* type and its doping with substitutional donors is easy and controllable up to a few 10^{19} cm^{-3}. However, the development of efficient GaN-based optoelectronic devices has long been hampered by the difficulty to dope it to *p* type. Akasaki *et al.*[1] first showed that magnesium is an efficient *p*-type dopant in GaN grown by metalorganics vapor phase epitaxy (MOVPE), provided that a post-growth treatment is used to electrically activate it. This was performed using low-energy electron bombardment in an electron microscope. Later, Nakamura *et al.*[2] showed that this could be more simply obtained by thermal annealing in a nitrogen atmosphere, and that the activation of magnesium results from the dissociation of some Mg-H complexes. On another hand, when Mg-doped GaN is grown by molecular beam epitaxy (MBE), this annealing step is not necessary.[3] Mg is today the only reliable *p*-type dopant in GaN, but its large Hall depth, around 160 meV,[4,5] necessitates large atomic concentrations [Mg], in the 10^{19} cm^{-3} range, leading to free hole densities (p) at room temperature saturating around 1 to 2×10^{18} cm^{-3}. A further increase of the Mg concentration, up to typically 1×10^{20} cm^{-3} leads to a strong decrease of the free hole concentration.[6–8] This is commonly interpreted as autocompensation due to an increased formation of N vacancies (V_N) and/or MgV_N or Mg_2V_N complexes,[6,7] following the decrease of the crystal's Fermi level with increasing Mg concentration.

Using transmission electron microscopy (TEM), we have recently observed[8,9] in Mg-doped GaN grown by MOVPE samples the formation of nanometer scale pyramidal inversion domains (PID's) for [Mg] higher than a few 10^{19} cm^{-3}. These pyramids have a hexagonal base which lies in the (0001) plane and with six $\{1\bar{2}13\}$ inclined facets. Actually, structural defects of similar shape, with a large size (up to 100 nm) were first observed in Mg-doped, high pressure grown, bulk GaN single crystals.[10,11] It is necessary to briefly recall literature results on structural defects appearing in highly Mg-doped GaN. Pyramidal defects observed in bulk and MOVPE-grown crystals have been ascribed to hollow cavities in Ref. 11. In the case of our MOVPE-grown samples, electron energy loss studies have shown no thickness variations between regions with and without defects, ruling out the possibility that PID's are empty, while the contrast reversal observed in dark field images indicates that they correspond to inversion domains.[9] Other authors report the presence of several kinds of structural defects in bulk Mg-doped GaN: spontaneously formed inversion domains superlattices[11] and dome-shaped defects filled with amorphous material or precipitates.[10] In MOVPE GaN with [Mg] higher than 10^{20} cm^{-3}, defects with complicated shapes corresponding to the coalescence of various PID's, or also columnar inversion domains have been reported too.[12] Another frequent observation in the literature is the formation of extended basal inversion domain boundaries.[7,11–14] These boundaries are atomically flat when formed on an N face, and facetted when formed from a Ga face,[14] in agreement with the orientation of PID's, which can be seen as closed inversion domain boundaries (inversely, a basal inversion domain can be seen as coalesced PID's). In summary, for Mg doping of GaN above a few 10^{19} cm^{-3}, the structural defects which form are mainly inversion domains. This can simply be a change of the polarity of the growing crystals or the appearance of closed pyramids with inverted polarity relative to the matrix. This last case corresponds to most of the highly Mg-doped MOVPE-grown samples that we have studied and is in agreement with the literature.[15,16]

From our TEM observations,[8] the size of the pyramidal defects agrees with previous reports[11] for bulk, high pressure-grown GaN.[17] In standard Mg-doped GaN grown by MOVPE on (0001) sapphire,[18] the defects are much smaller (2–6 nm). However, when Mg is introduced during MOVPE growth on inclined facets to planarize surfaces in our epitaxial lateral overgrowth (ELO) procedure,[19] various intermediate sizes may be observed.

In this work, a detailed TEM study of the pyramidal defects appearing in Mg-doped GaN is performed, allowing us to propose a structural model at the atomic level. Previously

proposed atomic models for inversion domains boundaries are also considered.[13,20]

In a second part, we shall see if the existence of such nanometer wide pyramidal inversion domains can be correlated to the abovementioned autocompensation problem. Indeed, whatever the investigating group, PID's appear for [Mg] in the mid 10^{19} cm^{-3} which corresponds to the onset of the free hole concentration saturation.[8,15–16]

II. EXPERIMENTAL DETAILS

Mg-doped GaN samples grown using various methods were investigated using TEM, Hall effect, and secondary ion mass spectroscopy (SIMS). The details about the different growth techniques may be found elsewhere [bulk,[17] MOVPE,[18] MBE (Ref. 3)]. TEM analyses, mostly cross-sectional, were performed using a 200 keV field emission gun (FEG) JEOL 2010 electron microscope equipped with an energy dispersive x-ray spectroscopy (EDX) Oxford ISIS attachment. The image simulations have been performed using the JEMS software package.[21] The following parameters have been used for simulations: a spherical aberration coefficient (Cs) of 0.5 mm, a beam half convergence of 0.68 mrad, and a defocus spread of 4.5 nm. The TEM objects were prepared by mechanical polishing and argon ion thinning.[9] Hall effect experiments were performed in the Van der Pauw geometry, using In or Au/Ni contacts. A Hall factor of unity is assumed (note that as frequently reported for Mg-doped GaN, data for low Mg concentrations, typically p lower than 10^{17} cm^{-3} at 300 K, are very noisy due to very low Hall mobility). Care was taken to perform every analysis, including SIMS, from the same piece of each studied wafer.

III. STRUCTURAL STUDIES

In MOVPE-grown samples, the size of the PID's is, in most cases, thinner than the TEM objects. This means that these defects are most of the time buried within the bulk, which may introduce some artifacts due to the interferences during high-resolution TEM (HRTEM) imaging. Therefore, we have used a bulk sample with large pyramidal defects to conduct the study of their atomic structure. But it is first necessary to verify that pyramidal defects in bulk and MOVPE-grown Mg-doped GaN are of the same nature. Such a large pyramidal defect in a bulk sample is shown in Fig. 1(a). Thickness fringes, which are running parallel to the object edge are not affected by the defect. Therefore, this defect is not an empty volume. Moreover, the absence of extra fringes in most of the defect area (extra fringes are only seen close to the defect's apex) indicates that the defect crosses the entire TEM object. Convergent beam electron diffraction (CBED) patterns from areas of the same thickness inside and outside the defect [Figs. 1(b) and 1(c)] clearly demonstrate a reversal of polarity between the defect and the matrix. A comparison with a simulated CBED pattern for an object thickness of 20 nm [Fig. 1(d)] leads to the schematic representation of polarity distribution shown in Fig. 1(e). In

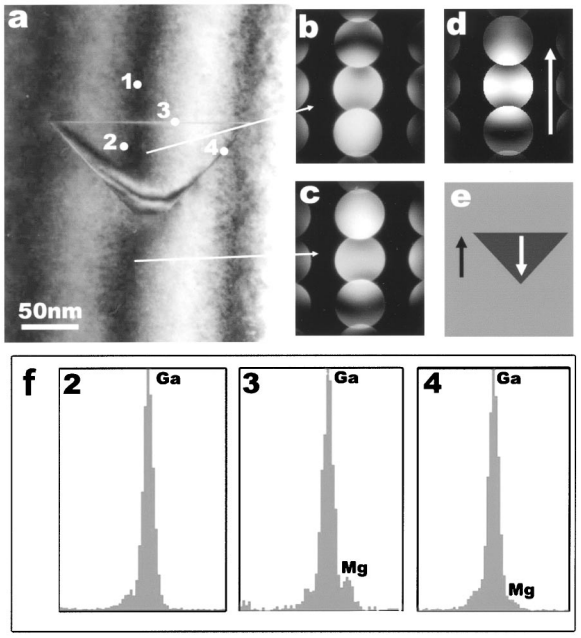

FIG. 1. (a) Bright field image of a large pyramidal defect in Mg-doped bulk GaN. The numbers show the different areas where EDX analyses have been performed. (b) Experimental CBED pattern from inside the pyramidal defect. (c) Experimental CBED pattern from the matrix. (d) Simulated CBED pattern for an object thickness of 20 nm. (e) Polarity distribution in the PID. The arrows in Figs. 1(d) and 1(e) show the [0001] positive direction. (f) EDX spectra from the points shown in (a).

Figs. 1(d) and 1(e), the arrows indicate the positive [0001] direction, i.e., point to the Ga face. Pyramidal defects are therefore inversion domains in both bulk and MOVPE-grown Mg-doped GaN.

The different configurations of inversion domain boundaries (IDB's) have been referred as ''head to head'' when the positive [0001] directions are pointing to the IDB and ''tail to tail'' when the negative $[000\bar{1}]$ directions are pointing to the IDB.[22] In PID's, which are closed inversion domains, the ''tail to tail'' IDB's are in the basal plane whereas ''head to head'' IDB's are in inclined $\{1\bar{2}13\}$ planes. The same configuration of IDB's is observed when a total reversal of polarity is induced by Mg doping in MBE and MOVPE-grown GaN films.[12–14]

To study the distribution of Mg in the PID's, EDX analysis using a 0.5 nm diameter probe have been performed on four different areas shown in Fig. 1(a): outside the defect in the matrix (point 1), in the center of the PID (point 2), in the basal inversion domain boundary (IDB) (point 3), and in the inclined IDB (point 4). Mg concentrations are below the detection limit in both the matrix and the center of the PID whereas Mg enrichment is clearly detected in the basal and also in the inclined IDB's [Fig. 1(f)]. The lower [Mg] detected in the inclined IDB's may be explained by the pyramidal shape of the PID's with the length of the inclined facet along the beam direction rapidly decreasing from the basal IDB to the apex of the pyramid. High resolution TEM has then been conducted to determine the atomic structure of

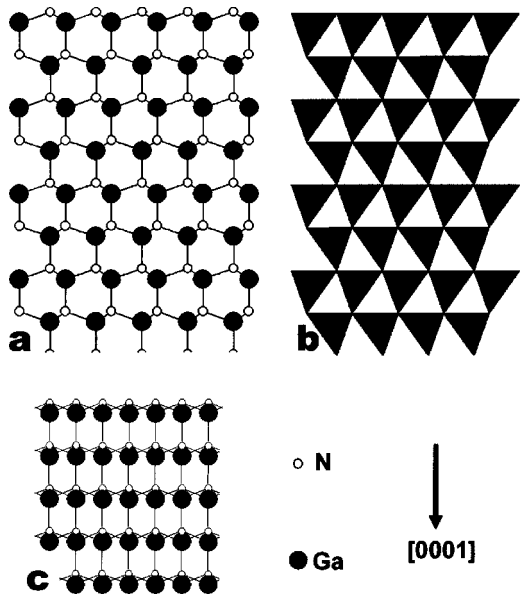

FIG. 2. (a) GaN structure projected along $[11\bar{2}0]$. (b) N tetrahedra representation of the GaN structure projected along $[11\bar{2}0]$. (c) GaN structure projected along $[10\bar{1}0]$.

these Mg-rich IDB's. We first focus on the basal IDB's.

Wurtzitze GaN structure can be described as a hexagonal stacking of N compact planes with Ga atoms filling one half of the tetrahedral sites of the N sublattice. In Fig. 2, the Ga atoms fill the tetrahedra pointing downward. In this representation, the positive [0001] direction also points downward. Mg being a substitutional atom of Ga, Mg enrichment may induce the formation of a N-Mg compound. Mg_3N_2, which is the only reported N-Mg compound, has an antibixbyite structure[23,24] (Fig. 3) which can be described as a face centered cubic stacking of N compact planes with Mg filling both up- and down-pointing tetrahedra of the N sublattice, with a filling factor of 3/4. Figures 3(a) and 3(c) are representations of a perfect antibixbyite structure. The actual structure of Mg_3N_2 is shown in Fig. 3(d) including distortions of N tetrahedra depending whether they are filled or not with Mg.[23,24]

We proposed a structural model (Fig. 4) which takes into account our experimental observations (Fig. 5). The right image in Fig. 5 is a HRTEM image along the $[11\bar{2}0]$ zone axis of a basal IDB for an object thickness of 13 nm and a defocus of 64 nm. In this image the PID is at the bottom and the matrix at the top. Image simulations for this zone axis show that for a thickness range from 8 to 20 nm and a defocus range from 60 to 70 nm, the white points in the images correspond to the position of N atomic columns. This image therefore reveals that the N sublattice is continuous across the basal IDB with just an increase of (0002) interplanar distances at the IDB location. The model for the basal IDB, which is proposed in Fig. 4 corresponds to the introduction of a monolayer of Mg_3N_2 [framed in Fig. 3(a)] in between two GaN crystals of reversed polarity. In the bottom GaN crystal, the N tetrahedra pointing downward are filled with Ga whereas in the upper crystal that are the tetrahedra pointing upward which are filled with Ga atoms. The transition between these two crystals is a Mg_3N_2 monolayer where both kind of tetrahedra are filled with Mg atoms (filling factor 3/4). It has to be noted that such a model corresponds,

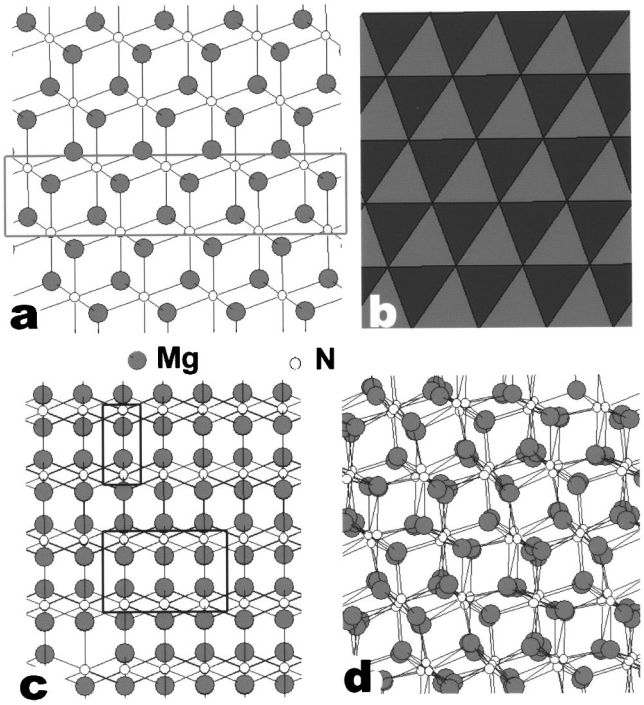

FIG. 3. (a) Mg_3N_2 in a perfect antibixbyite structure projected along [110]. The cell that is used for building the model for basal IDB's is framed. (b) N tetrahedra in perfect Mg_3N_2 antibixbyite structure projected along [110]. (c) Mg_3N_2 in a perfect antibixbyite structure projected along [112]. The cells that are used for building the models for inclined IDB's are framed. (d) Actual Mg_3N_2 structure projected along [110].

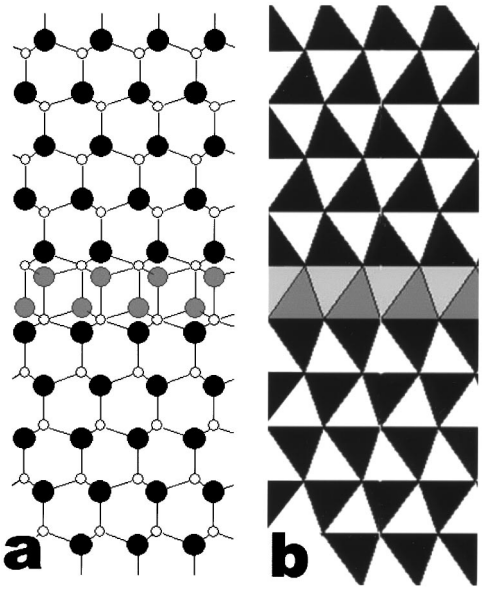

FIG. 4. Model for the basal IDB projected along the $[11\bar{2}0]$ direction of GaN. (a) Atomic representation, (b) N tetrahedra representation. Tetrahedra filled with Ga are in black and tetrahedra filled with Mg are in gray.

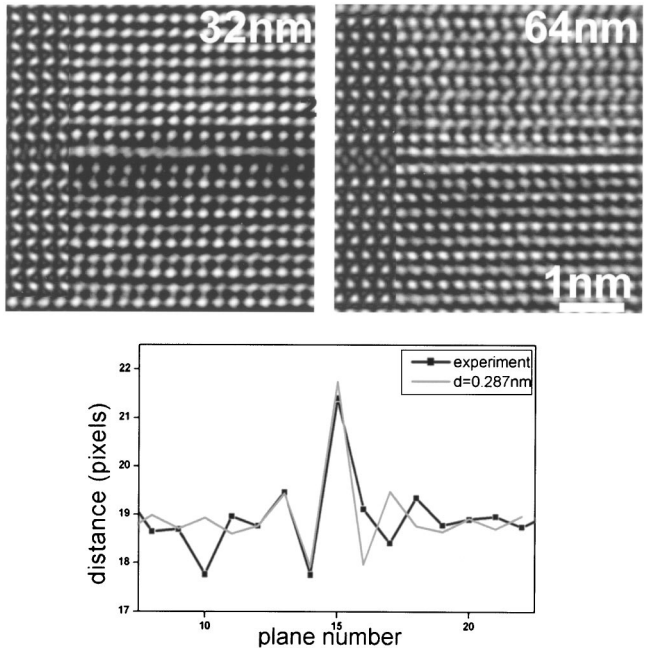

FIG. 5. HRTEM images along $[11\bar{2}0]$ zone axis of a basal IDB for an object thickness of 13 nm and defoci of 32 and 64 nm. The left part of each images are simulated images for the model proposed in Fig. 4. The graph shows the distances between basal planes measured in the experimental image (black curve) and in the simulated image with a basal plane distance in the IDB of 0.287 nm (light gray).

along $[0001]_{GaN}$, to the replacement of one Ga hexagonal compact plane by two Mg planes with a filling factor of 3/4, which keep the neutrality of the crystal. Image simulations for this structural model have been performed for a sample thickness of 13 nm and defoci of 32 and 64 nm (left parts of each image) and compared to experimental images. A very good fit between simulated and experimental images is observed taking into account the simplicity of the model that we proposed. In fact, the Mg_3N_2 monolayer introduced in the IDB for the simulation is of a perfect antibixbyite structure with all the tetrahedra (with or without Mg) having the same size, which is not the case in the actual Mg_3N_2 structure. In the model, the Mg atoms are kept at the center of the N tetrahedra. The strain due to the introduction of this Mg_3N_2 monolayer has also been limited to the IDB whereas it certainly extends to the surrounding GaN layers.

In building the atomic model, we have used for simulations the following interatomic distances: the in-plane N interatomic distances are those of GaN whereas the distances between N basal planes (d) are those of Mg_3N_2. The antibixbyite unit cell corresponds to four face centered cubic basic unit cells. Therefore, using the recently determined lattice parameter of Mg_3N_2 ($a_{Mg_3N_2}=0.9528$ nm) (Ref. 24)

$$d=\frac{a_{Mg_3N_2}}{2\sqrt{3}}=0.2873 \text{ nm}.$$

A comparison between the basal planes distances measured in the simulated and experimental images is also shown in Fig. 5. The values obtained for $d=0.2873$ nm (light gray curve) correctly fit the experimental values (dark curve) within the error limit. In fact, the fit is correct for $d=0.28-0.29$ nm. With smaller in-plane and similar out-of-plane atomic distances, the volume of the Mg_3N_2 cell volume is then reduced as compared to bulk material.

Based on total energy calculations, Northrup[19] proposed another model for the basal IDB. As with ours, this model takes into account an Mg enrichment of the basal IDB and the continuity of the N sublattice across the IDB. But, while the IDB is formed by a double layer of Mg corresponding to a Mg_3N_2 stacking in our model, in Northrup's model the IDB is formed of a single Mg layer in cubic position. From his calculations, this configuration should be the most stable one. We have performed images simulations for this model too. Figure 6 shows a comparison between simulated images (left parts of each image) and the same experimental images as in Fig. 5. Qualitatively, our model gives a better fit to the experimental images. This is clearest in the image at a defocus of 32 nm. The white points, which are seen at the IDB location in the experimental image, are not reproduced in the simulation. Nevertheless, these considerations are qualitative and it is difficult to definitively conclude from our data, since the Mg atoms are not directly seen in the images due to an insufficient spatial resolution of our TEM. Some other structural models have also been tested but with a poor fit between simulated and experimental images.[8]

Inclined IDB's are parallel to $\{1\bar{2}13\}$ planes so they are viewed edge-on for HRTEM images in $\langle 1\bar{1}00\rangle$ zone axis.

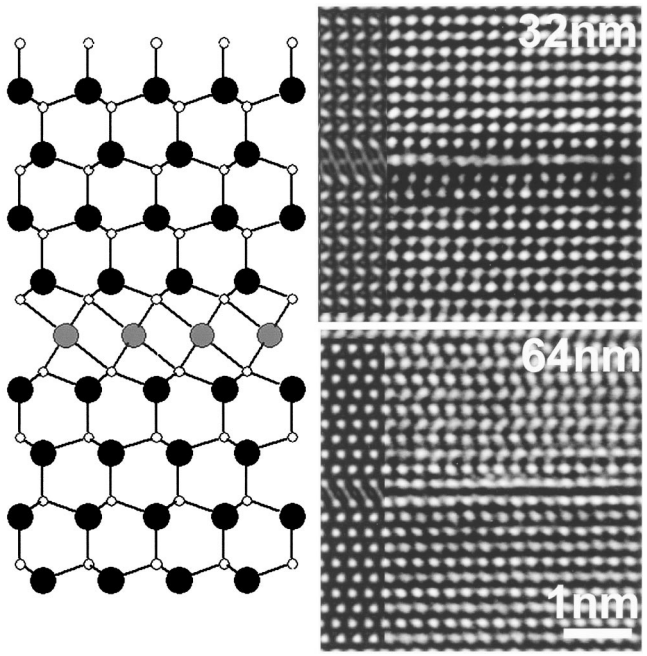

FIG. 6. Atomic model for the basal IDB as proposed by Northrup (Ref. 20). HRTEM images along $[11\bar{2}0]$ zone axis of a basal IDB for an object thickness of 13 nm and defoci of 32 and 64 nm. Left part of each images are simulated images for this model.

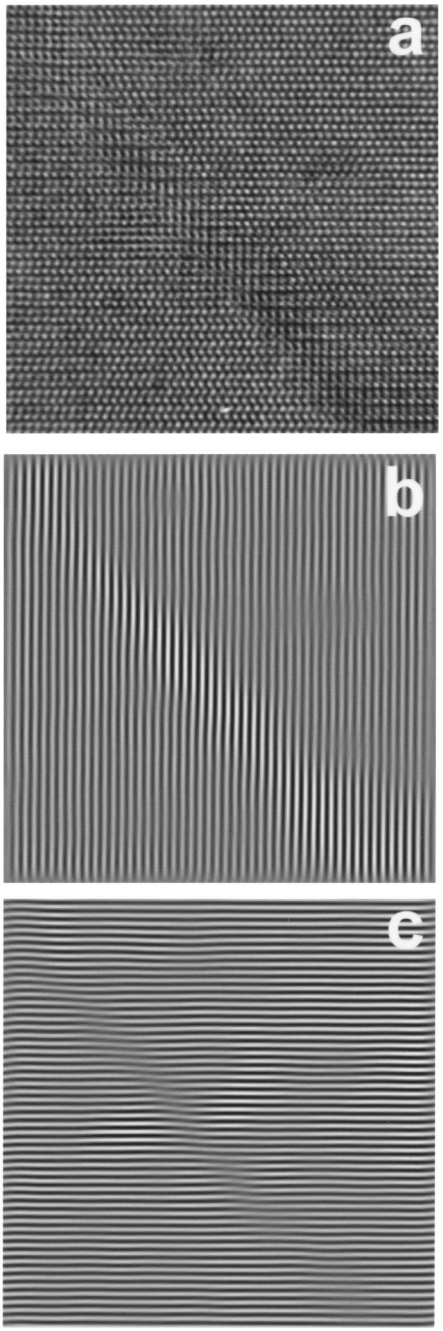

FIG. 7. (a) HRTEM image ($[11\bar{2}0]$ zone axis) of an inclined IDB; Fourier filtered images of (a) using $(1\bar{1}00)$ (b) and (0002) (c) spots.

The interreticular distances for $\{11\bar{2}0\}$ planes (0.159 nm) are smaller than the resolution of our TEM at Scherzer defocus and lattice resolution is only obtained thanks to the high coherency of the FEG electron beam, which results to an information limit of 0.14 nm. Nevertheless, simulations show that it is difficult to directly interpret the images along $\langle 1\bar{1}00\rangle$ zone axis in terms of atomic positions. Therefore, in a first step, inclined IDB's have been observed along $\langle 11\bar{2}0\rangle$ zone axis. Figure 7(a) is a $[11\bar{2}0]$ HRTEM image of such an inclined IDB for an object thickness around 10 nm and a defocus of 64 nm; N atomic columns are seen in white. Figures 7(b) and 7(c), which are Fourier filtered images of Fig. 7(a) using (0002) and $(1\bar{1}00)$ spots respectively, show that there is no translation of basal and vertical N planes between the PID's and the matrix. The only strains are detected at the inclined IDB location. Observation along $[1\bar{1}00]$ zone axis (Fig. 8) demonstrates that inclined IDB's, which have an average orientation $(1\bar{2}13)$, are in fact formed by successive $(1\bar{2}12)$ and $(1\bar{2}16)$ segments. It should be noted that to obtain an average $(1\bar{2}13)$ direction for the inclined IDB, the sum of the length of the $(1\bar{2}12)$ segments projected on the *c* axis should be 3 times that of the $(1\bar{2}16)$ segments. Assuming that, as in the basal IDB's, the transition between the two GaN crystals with reversed polarities is formed by the insertion of Mg_3N_2, and taking into account the continuity of the N sublattice, we propose the model shown in Fig. 9 for the $(1\bar{2}12)$ IBD. The Mg_3N_2 brick, which is introduced in the IDB is framed in Fig. 3(c). In this model, two N tetrahedra filled with Mg (filling factor 3/4) replace two N tetrahedra with only one filled with Ga therefore the crystal neutrality is maintained. The comparison of the simulated and experimental images for the model we proposed for an object thickness of 5 nm and defoci of 36, 56, and 66 nm are shown in Fig. 9. The fit between simulations and experience is qualitatively correct. The differences between the simulated and experimental images for this model may also be explained by its simplicity. In fact, we just have introduced Mg_3N_2 by filling pointing upward and downward tetrahedra with Mg (filling factor$=3/4$) in the $(1\bar{2}12)$ IDB keeping GaN interatomic distances. Nevertheless, this model may be considered as basically correct. Another model has already been proposed[13] for $(1\bar{2}12)$ IBD. In this model, it is the Ga sublattice rather than the N sublattice which is continuous across the IDB. Image simulations have also been performed to test it. The fit between simulated and experimental images (not shown) is definitively worst.

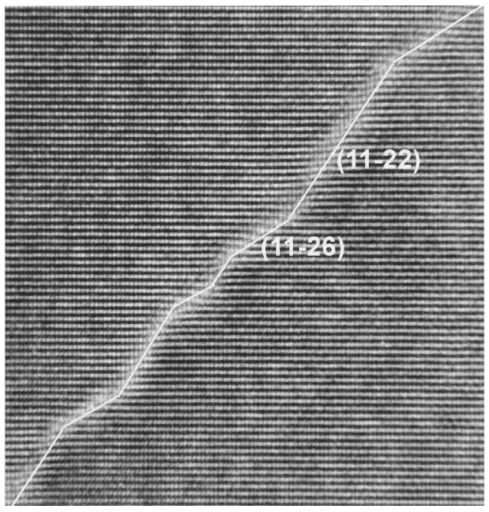

FIG. 8. HRTEM image ($[10\bar{1}0]$ zone axis) of an inclined IDB. $(1\bar{2}12)$ and $(1\bar{2}16)$ segments are indicated.

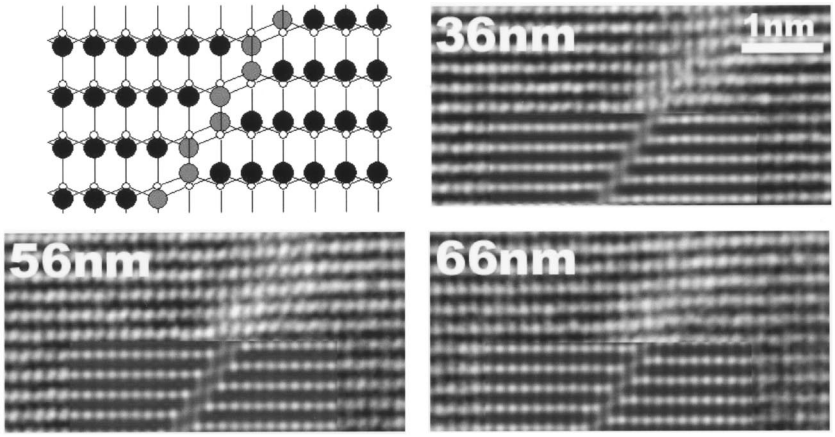

FIG. 9. Proposed model for the $(1\bar{2}12)$ inclined IDB, projected along the $[10\bar{1}0]$ direction of GaN. Experimental and simulated HRTEM images ($[10\bar{1}0]$ zone axis) for an object thickness of 5 nm and defoci of 36, 56, and 66 nm.

It is then possible to build a model for the $(1\bar{2}16)$ IDB which is also formed by the insertion of Mg_3N_2 in the IDB and which keeps the continuity of the N sublattice (Fig. 10). The Mg_3N_2 brick, which is introduced in the IDB is also framed in Fig. 3(c). The crystal neutrality is also maintained. With the same limitations as for the $(1\bar{2}12)$ IDB, the fit between the experimental and simulated images for an object thickness of 5 nm and different defoci (36, 56, and 66 nm) is correct (Fig. 10).

The main result about the structure of the PID's obtained from the above determination of the IDB's structures is that the N sublattice is not affected by the defect. We propose a model for IDB's where there is only a change of the kind of tetrahedra which are filled with Ga in and outside the defect. The transition between the two regions is formed by the local insertion of Mg_3N_2 in which both kinds of tetrahedra are filled with Mg. The only strains in this structure are localized at the IBD's. With such a structure, there is no need for dislocation at the intersection of basal and inclined IDB's.

IV. INFLUENCE OF PYRAMIDAL INVERSION DOMAINS ON FREE HOLE CONCENTRATIONS

PID's appear in highly Mg-doped MOVPE-grown GaN in a doping range where autocompensation of Mg acceptors begins. In the first part of this paper, a structural model was proposed for these defects: the PID's are pyramidal inversion domain of varying size, but that are typically very small (2.5 to 6 nm wide) in MOVPE-grown *p*-type GaN. The inversion domain boundary consists of a molecular plane of Mg_3N_2 in the basal plane, whereas the inclined facets of the PID's are also composed of Mg_3N_2 bricks. Using this structural model, we shall now try to evaluate the influence of these defects on the free hole concentrations.

Figure 11(a) shows the room temperature hole concentration *p*, measured by Hall effect, of a series of Mg-doped GaN samples grown by MOVPE, as a function of the global magnesium content [Mg] measured by SIMS. An MBE-grown sample is also shown. Up to $[Mg]\sim 10^{19}$ cm^{-3}, *p* increases with [Mg], as expected, then it saturates to $p\approx 1-2\times 10^{18}$ cm^{-3}. At higher Mg content $[Mg]>6\times 10^{19}$ cm^{-3}, a strong drop in free hole concentration is observed. This typical behavior has already been reported for MOVPE-grown Mg-doped GaN, with *p* and [Mg] values only slightly varying among laboratories.[6,7]

The solid line in Fig. 11(a) is the calculated room temperature free hole density assuming negligible compensation.[25] The parameters used are $E_A=160$ meV and $m_h=0.8m_0$ for each valence band (since the three valence bands of GaN are very near in energy, we take this into account using suitable Boltzmann factors[6]). The spin degeneracy of the acceptor β is set to 2, since we have not observed any acceptor excited states energetically closed to the ground state in our temperature dependant luminescence studies of acceptors in GaN.[26] Actually, this set of parameters allows us to satisfactorily account for the Hall effect in weakly compensated Mg-doped GaN in the 150–450 K temperature range, leading to acceptor concentrations in good agreement with their SIMS determination (not shown). As Fig. 11(a) shows, such a calculation is in good agreement with the free hole density in the low Mg doping range, but

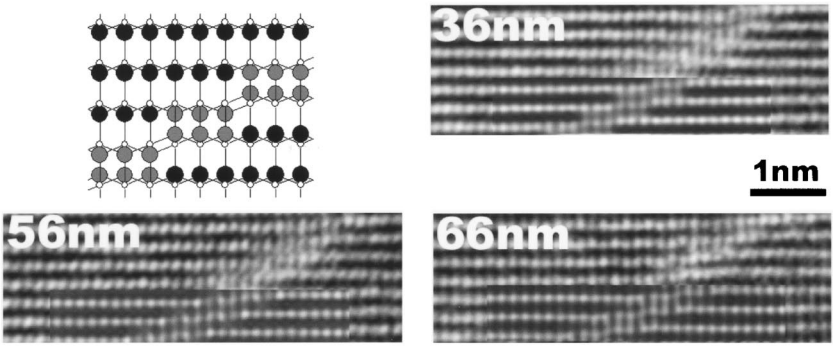

FIG. 10. Model for $(1\bar{2}16)$ inclined IDB, projected along the $[10\bar{1}0]$ direction of GaN. Experimental and simulated HRTEM images ($[10\bar{1}0]$ zone axis) for an object thickness of 5 nm and defoci of 36, 56, and 66 nm.

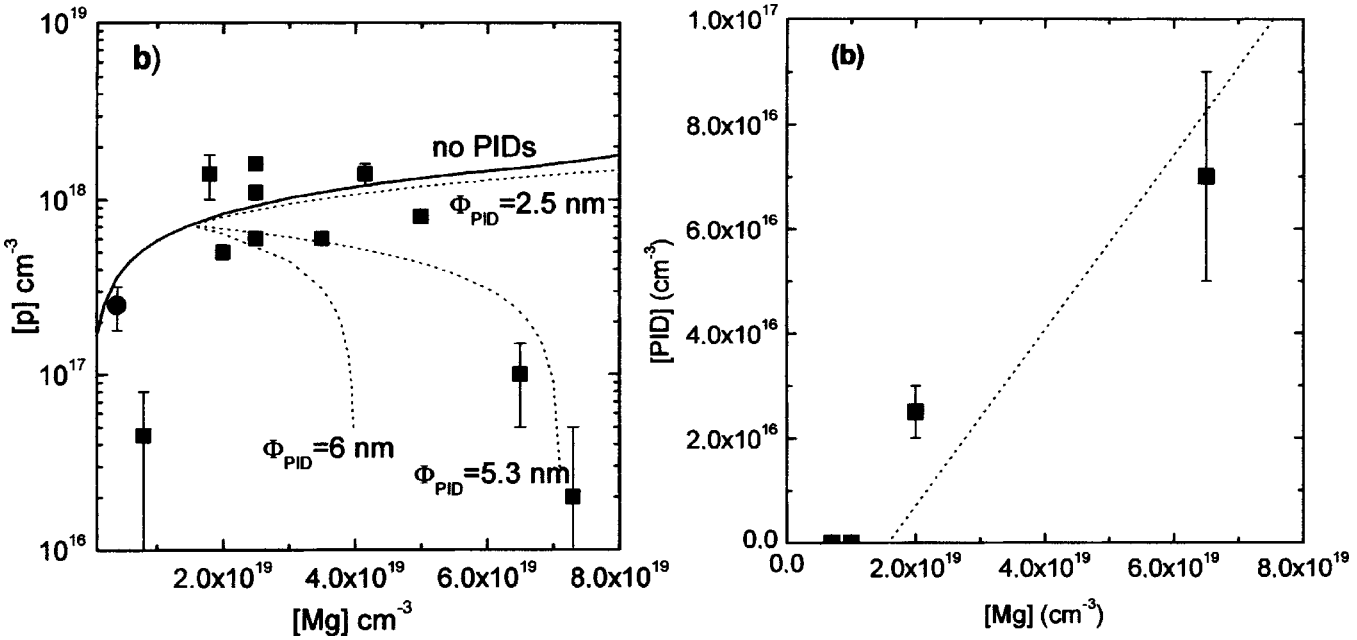

FIG. 11. (a) Mg concentration dependence of the room temperature hole concentration in Mg-doped GaN. Squares are MOVPE-grown samples; the circle corresponds to an MBE-grown sample. (b) Pyramidal inversion domain concentration as a function of Mg concentration in some of the samples of Fig. 11(a).

cannot account for the decrease of free hole density at high Mg concentration. As mentioned in Ref. 6, the introduction of a constant concentration of compensating donors (typically N_D in the $10^{17}-10^{18}$ cm^{-3} range) cannot give a better agreement. As mentioned in the Introduction, autocompensation has been interpreted as due to V_N or (V_N-Mg) complexes formation related to the decrease of the crystal's Fermi level.[6,7] In the following, we shall, however, investigate the possible role of PID's in this limitation of the free hole density.

Figure 11(b) shows the PID density [PID] measured by TEM in some of the samples of Fig. 11(a). No PID's are detected when $[\mathrm{Mg}] \leqslant 10^{19}$ cm^{-3}, they begin to be observed when $[\mathrm{Mg}] = 2\times10^{19}$ cm^{-3} and their density increases with Mg concentration. Note that a similar increase of PID density with Mg doping has been reported in Ref. 15. Lower PID's densities than in our samples are reported, but their density is again in the 10^{16} cm^{-3} range and, interestingly, these data are also in agreement with PID appearance when $[\mathrm{Mg}] \geqslant 1\times10^{19}$ cm^{-3}.

Since our data only concern the domain $[\mathrm{Mg}] < 1\times10^{20}$ cm^{-3}, we shall assume for simplicity that the increase of PID's density with [Mg] is linear in this range. Thisis shown as a dotted line in Fig. 11(b), corresponding to $[\mathrm{PID}] \approx 1.67\times10^{-3}$ ($[\mathrm{Mg}] - 1.5\times10^{19}$) above a threshold value of $[\mathrm{Mg}] = 1.5\times10^{19}$ cm^{-3}. (Of course, the range is limited, since PID's cannot consume more magnesium than is present in the crystal.) The areal density of Ga sites in GaN is 1.136×10^{15} cm^{-2}. The PID's in the MOVPE-grown samples studied in Fig. 11 are between 2.5 and 6 nm wide. Assuming the atomic structure proposed in this work, each PID then consumes between ~170 and 970 atoms of magnesium. We can then calculate the free hole density in our samples, using the fact that the number of acceptors N_A is now the total magnesium concentration *minus* those consumed in PID's. This is shown as dashed lines in Fig. 11(a), for 2.5 or 6 nm wide PIDS. The experimental data are encircled by the calculated curves. It should be noticed that if PID's are all large (width 6 nm), all magnesium atoms should be consumed by PID's for an Mg concentration as low as 4×10^{19} cm^{-3} [under the assumption of the linear variation of PID density shown in Fig. 11(b)]. As an indication, we show in Fig. 11(a) that it is possible to account for the free hole density decrease at high Mg doping in our samples using a suitable average PID size ($\Phi \sim 5.3$ nm). We also mention that curves as shown in Fig. 11(a) can be generated using a higher β value ($\beta \sim 4$, i.e., near zinc blende case), as sometimes proposed in the literature, by using a slightly larger hole mass of $1.1m_0$. The results in Figs. 11 show that the high concentration of PID's in MOVPE-grown Mg-doped GaN may account for the self-compensation phenomenon in *p*-type GaN. *A minima*, it shows that the presence of PID's has at least to be considered when studying this self-compensation problem. This conclusion is in agreement with the results of Figge *et al.*,[16] showing a strong decrease of free hole density correlated with the appearance of PID's in Mg-doped samples, and those of Hansen *et al.*,[15] who report an increase of the series resistance of nitride laser diodes with increasing PID density in the *p*-type electrode.

CONCLUSIONS

A detailed transmission electron microscopy of pyramidal defects formed in Mg-doped GaN confirms that they are inversion domains. A high-resolution microscopy study per

formed on large defects as formed in bulk Mg-doped GaN allows us to propose that the inversion domain boundaries are likely composed of Mg_3N_2 bricks. This is in agreement with an Mg enrichment of these boundaries experimentally observed. In MOVPE-grown, Mg-doped GaN, the pyramidal inversion domains are nanometer wide, and appear for Mg concentrations in the low to mid 10^{19} cm^{-3} range. Their concentration is large enough to play a significant role in the autocompensation in Mg-doped GaN grown by MOVPE.

ACKNOWLEDGMENTS

M. Albrecht (University of Erlangen) is acknowledged for fruitful discussions and experimental work. We also thank F. Jomard (CNRS Bellevue) and C. Grattepain (Thomson-LCR, Corbeville) for SIMS measurements and I. Grzegory and S. Porowski (Unipress, Warsaw) for providing the bulk GaN sample studied. This work has been supported in part by EEC Contracts No. HPRN-CT-1999-00040 (IPAM).

*Email address: pv@crhea.cnrs.fr

[1] I. Akasaki, H. Amano, Y. Koide, K. Hiramatsu, and N. Sawaki, J. Cryst. Growth **98**, 209 (1989).

[2] S. Nakamura and G. Fasol, *The Blue Laser Diode* (Springer-Verlag, Berlin, 1997), and references therein.

[3] N. Grandjean, J. Massies, M. Leroux, and P. Lorenzini, Appl. Phys. Lett. **72**, 82 (1998).

[4] W. Götz, N. M. Johnson, J. Walker, D. P. Bour, and R. A. Street, Appl. Phys. Lett. **68**, 667 (1996).

[5] H. Nakayama, P. Hacke, M. R. H. Kahn, T. Detchprohm, K. Hiramatsu, and N. Sawaki, Jpn. J. Appl. Phys. **35**, L282 (1996).

[6] U. Kaufmann, P. Schlotter, H. Obloh, K. Köhler, and M. Maier, Phys. Rev. B **62**, 10 867 (2000).

[7] L. T. Romano, M. Kneissi, J. E. Northrup, C. G. Van de Walle, and D. W. Treat, Appl. Phys. Lett. **79**, 2734 (2001).

[8] M. Leroux, P. Vennéguès, S. Dalmasso, M. Benaissa, E. Feltin, P. de Mierry, B. Beaumont, B. Damilano, N. Grandjean, and P. Gibart, Phys. Status Solidi A **192**, 394 (2002).

[9] P. Vennéguès, M. Benaissa, B. Beaumont, E. Feltin, P. de Mierry, S. Dalmasso, M. Leroux, and P. Gibart, Appl. Phys. Lett. **77**, 880 (2000).

[10] J. A. Kozubowski, J. Borysink, H. W. Zandbergen, I. Grzegory, J. L. Weyher, and S. Porowski, in *Proceedings of the Xth Conference on Electron Microscopy in Solids* (Serock, Poland, 1999), p. 413.

[11] Z. Liliental-Weber, M. Benamara, J. Washburn, I. Grzegory, and S. Porowski, Phys. Rev. Lett. **83**, 2370 (1999); Z. Liliental-Weber, J. Jasinski, M. Benamara, I. Grzegory, S. Porowski, D. J. H. Lampert, C. J. Eiting, and R. D. Dupuis, Phys. Status Solidi B **228**, 345 (2001).

[12] P. Vennéguès, M. Benaissa, B. Beaumont, B. Damilano, N. Grandjean, *Microscopy of Semiconducting Materials 2001 Conference*, Institute of Physics Conferences Series No. 169 (Institute of Physics, Bristol, 2001), p. 307.

[13] L. T. Romano, J. E. Northrup, A. J. Plak, and T. H. Myers, Appl. Phys. Lett. **77**, 2479 (2000).

[14] N. Grandjean, A. Dussaigne, S. Pezzagna, and P. Vennéguès, J. Cryst. Growth **251**, 460 (2003).

[15] M. Hansen, L. F. Chen, S. H. Lim, S. P. Denbaars, and J. S. Speck, Appl. Phys. Lett. **80**, 2469 (2002).

[16] S. Figge, R. Kröger, T. Böttcher, P. L. Ryder, and D. Hommel, Appl. Phys. Lett. **81**, 4748 (2002).

[17] E. Litwin-Staszewska, T. Suski, I. Grzegory, S. Porowski, P. Perlin, J. L. Robert, S. Contreras, D. Wasik, A. Witowski, D. Cote, and B. Clerjaud, Phys. Status Solidi B **216**, 567 (1999), and references therein.

[18] B. Beaumont, M. Vaille, P. Lorenzini, P. Gibart, T. Boufaden, and B. El Jani, MRS Internet J. Nitride Semicond. Res. **1**, 17 (1996); S. Haffouz, B. Beaumont, M. Leroux, M. Laügt, P. Lorenzini, P. Gibart, and L. G. Hubert-Pfalzgraf, *ibid.* **2**, 37 (1997).

[19] P. Vennéguès, B. Beaumont, V. Bousquet, M. Vaille, and P. Gibart, J. Appl. Phys. **87**, 4175 (2000).

[20] J. E. Northrup, Appl. Phys. Lett. **82**, 2278 (2003).

[21] URL http://cimewww.epfl.ch/people/stadelmann/jemsWebSite/jems.html

[22] J. C. Choul Kim and E. Goo, J. Am. Ceram. Soc. **73**, 877 (1990).

[23] J. David, Y. Laurent, and J. Lang, Bull. Soc. Fr. Mineral. Cristallogr. **94**, 340 (1971).

[24] D. E. Partin, D. J. William, and M. O'Keffe, J. Solid State Chem. **132**, 56 (1997).

[25] J. S. Blakemore, *Semiconductor Statistics* (Pergamon Press, Oxford, 1962).

[26] M. Leroux, N. Grandjean, B. Beaumont, G. Nataf, F. Semond, J. Massies, and P. Gibart, J. Appl. Phys. **86**, 3721 (1999).